Exploring proximity effects and large depth of field in helium ion beam lithography: large-area dense patterns and tilted surface exposure

Ranveig Flatabø,[1,2,a)] Akshay Agarwal,[2] Richard Hobbs,[2,3] Martin M. Greve,[1] Bodil Holst,[1] and Karl K. Berggren[2,b)]

[1)] *University of Bergen, Department of Physics and Technology, Allégaten 55, 5007 Bergen, Norway*

[2)] *Research Laboratory of Electronics, Massachusetts Institute of Technology, MA 02139, USA*

[3)] *Centre for Research on Adaptive Nanostructures and Nanodevices (CRANN) & Advanced Materials Bio-Engineering Research Centre (AMBER), School ofChemistry, Trinity College Dublin, Dublin 2, Ireland.*

Helium ion beam lithography (HIL) is an emerging nanofabrication technique. It benefits from a reduced interaction volume compared to that of an electron beam of similar energy, and hence reduced long-range scattering (proximity effect), higher resist sensitivity and potentially higher resolution. Furthermore, the small angular spread of the helium ion beam gives rise to a large depth of field. This should enable patterning on tilted and curved surfaces without the need of any additional adjustments, such as laser-auto focus. So far, most work on helium ion beam lithography has been focused on exploiting the reduced proximity effect to reach single-digit nanometer resolution, and has thus been concentrated on single-pixel exposures over small areas. Here we explore two new areas of application. Firstly, we investigate the proximity effect in large area exposures and demonstrate HIL's capabilities in fabricating precise high-density gratings on large planar surfaces (100 μm × 100 μm, with pitch down to 35 nm) using an area dose for exposure. Secondly, we exploit the large depth of field by making the first HIL patterns on tilted surfaces (sample stage tilted 45°). We demonstrate a depth of field greater than 100 μm for a resolution of about 20 nm.

Keywords: helium ion beam lithography, proximity effects, depth of field, large-area exposures

[a)]Electronic mail: ranveig.flatabo@uib.no

[b)]Electronic mail: berggren@mit.edu

I. INTRODUCTION

The helium ion beam microscope (HIM) was commercialized in 2006[1]. An edge-resolution of 0.24 nm[2,3] has been demonstrated and HIM has been widely used for high resolution imaging, see *e.g.*[4–6]. Milling with helium ions for high resolution material modification is also becoming a well-established technique[7–11]. A less common use for HIM is resist-based lithography[12,13]. Lithography with a scanning helium ion beam, rather than an electron beam, benefits from a significant reduction in beam interaction volume for a given energy. For lithography purposes, this results in reduced long-range scattering (proximity effects) and increased resist sensitivity. Additionally, the small angular spread of the helium ion beam gives rise to a large depth of field[14,15] and hence large focus tolerance in nanofabrication.

Until now, work on helium ion beam lithography (HIL) has mostly been focused on reaching single-digit nanometer resolution, and has thus been concentrated on single-pixel exposures over small areas[12,13,16–18]. Resolvable 4 nm half-pitch lines in hydrogen silsequioxane (HSQ) have been demonstrated, and 8 nm half-pitch lines in 12 nm thick HSQ have been written over an area of 1 μm × 1 μm[16]. Recently, Shi et al.[17] fabricated 6 nm wide lines with 6 nm half-pitch in a methanofullerene derivative of C_{60}. In 2009 Sidorkin et al.[12] wrote 6 nm dots with a 14 nm pitch in (5 nm thick) HSQ over an area of 15 μm × 15 μm. The cornerstone in charge particle lithography, electron beam lithography (EBL), has realized dots in (negative tone) PMMA with a diameter of 1.7 nm and a pitch of 10.7 nm in a 4 μm × 4 μm write field[19]. This was accomplished using a 200 keV aberration-corrected EBL tool. Due to the thin films (resist and substrate) used for the exposures and the use of a high-energy-aberration-corrected EBL, no proximity effect correction was needed. In conventional EBL significant efforts have been made to find methods that compensate for the inherent proximity effects, such as dose modification within the design and shape modification, see *e.g.*[20–22].

High-density exposures over larger areas are of potential interest in *e.g.* diffractive elements, plasmonics, and electronics[23,24]. The lithographic point spread function of the helium ion beam is dominated by forward scattering[13,25]. This effectively means that the input CAD

design should match the exposed pattern for a known ion distribution and pixel size (print true to size). Further, for a given spot size, the convergence angle in the HIM is smaller than in an electron microscope, resulting in a larger depth of field. For example, Zeiss states that HIM has 5 -10 times larger depth of field than FE-SEM[26]. The minute long-range scattering combined with the large depth of field in HIM, gives a large focus tolerance for planar nano-lithography and fabrication.

The large depth of field can also address another challenge in nanofabrication, namely patterning on curved or tilted surfaces, or over surface topography. This can enable high resolution patterning of lenses or optical fibers[27,28] and be used to functionalize surfaces with tilted nanostructures[29,30] *etc.* Curved or tilted surfaces can readily be printed using a flexible stamp in nanoimprint lithography[31], but is extremely challenging without a dynamic focus correction in EBL[30]. So far no one has investigated the use of the large depth of field in HIM for HIL applications.

Here, we present two sets of measurements. Firstly we investigate the promiximity effects in large area exposures and demonstrate HIL's capabilities in fabricating precise, true to size, high-density gratings on planar surfaces. The gratings are exposed using an area dose density and hence have a non-zero width in the input CAD-file. Secondly, we measure the depth of field for various working distances, and pattern single-pixel lines while having the sample stage tilted 45° (Figure 1). This demonstrates (a) the large focus tolerance in HIL and (b) that HIL can be used to pattern on tilted and curved surfaces with high resolution without the need of any beam corrections such as a laser-auto focus.

II. EXPERIMENTAL

The helium ion microscope (Orion, Carl Zeiss SMT) used in this work was equipped with a 16-bit pattern generator (Elphy Multibeam, Raith Nanofabrication). All exposures were done in HSQ (2 % Dow Corning XR-1541) on silicon wafers. The resist was spin-coated onto the wafer at 6000 rpm for 1 minute. No adhesion promoter was used. To avoid thermal crosslinking, the resist was not baked. The thickness was measured using a reflectometer and was found to be approximately 30 nm. We used salty development[32], consisting of 1 % NaOH and 4 % NaCl in de-ionized water (weight to volume percentage). The samples were immersed in the developer at room temperature for 4 minutes, then immediately rinsed in

de-ionized water for 1.5 minutes and finally rinsed with IPA (propan-2-ol) and dried using pressurized nitrogen. The samples were characterized using FE-SEM with an acceleration voltage of 3 kV and an aperture of 20 μm, and the HIM using a landing energy of 30 keV and 10 μm aperture.

A. Exposure parameters

Small unexposed regions in designs are extremely sensitive to proximity effects[20–22]. To quantify the proximity effects in HIL, we exposed a 1 μm × 1 μm square in HSQ and left four windows in the center open. The width of the windows was either 40 nm or 30 nm (Figure 2), and the gap between the windows was half the size of the windows, namely, 20 nm or 15 nm. The exposure details are given in Table I.

The large-area gratings on planar surfaces were fabricated using an area dose density *i.e.* the lines were defined as rectangles with a width of 16 nm. The pitch was 50 nm, 40 nm or 35 nm. The beam was focused at a relatively long working distance ($\sim$ 9 mm). This was done to (a) get a larger depth of field and (b) increase the maximum write field. The HIM was not equipped with a laser interferometric stage and hence the largest area one can write without stitching errors is limited by the area written by beam deflection (write field). Using a 2 nm pixel size, the maximum write field of the 16-bit pattern generator is 100 μm × 100 μm. The write-time of the 100 μm × 100 μm grating was about 1.75 hours.

As discussed in Sec. I, the depth of field in the HIM is superior to that of an EBL tool (without a laser-auto focus). To demonstrate and estimate the large depth of field, and HIL's capabilities to pattern over surface topography or on curved or tilted surfaces, we exposed gratings (50 μm × 100 μm) while having the stage tilted 45°, as illustrated in Figure 1. The depth of field scales with the working distance, *i.e.* the larger the working distance, the larger the depth of field. Therefore, we focused the beam at a working distance of (a) $\sim$ 15 mm and (b) $\sim$ 27 mm. As the working distance was increased, the spot size also increases, and to accommodate this loss in resolution we exposed single pixel lines and increased the pixel size. In addition, we set the spot number to 5. The spot number sets the strength of the condenser lens and hence the beam crossover above the aperture. A larger spot number gives a smaller angular spread of the beam, and a larger depth of field. It can be increased beyond 5, but it comes at the cost of beam current. Details on exposure parameters are

given in Table I. A 10 μm aperture was used, but it should be noted that a 5 μm aperture is available in standard HIM instruments. Using a 5 μm aperture should decrease the angular spread of the beam and hence give an even larger depth of field. However, by reducing the aperture, the beam current is reduced and hence the write-time increased. To keep the write-time down, a 10 μm aperture was used, although with an increased spot number.

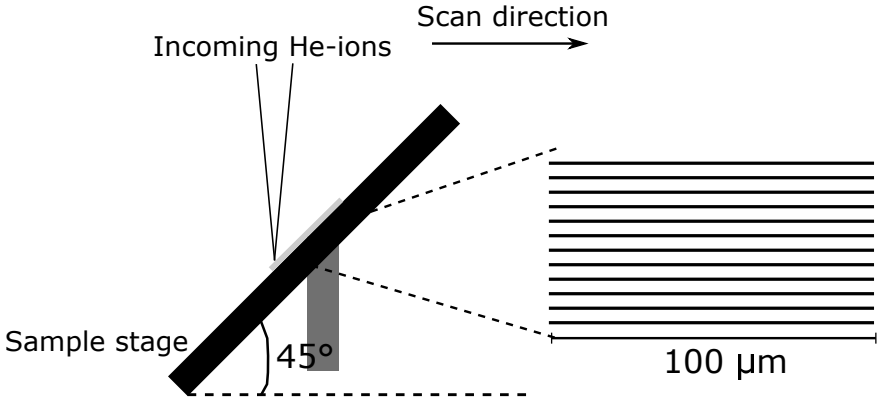

Figure 1. Illustration of HIL on a 45° tilted sample surface. The exposed pattern is 100 μm long.

The depth of field was also measured using HIM images. The pixel size in each image was 3.5 nm (1024×1024 resolution and 3.5 μm field of view), and the width of the feature in focus was 5 pixels for all working distances (6 mm, 10 mm and 15 mm). Defocus was defined as the condition when the width of the feature imaged became 3 times it's original width *i.e.* 15 pixels. This definition of defocus originates from the description of the Rayleigh length of a Gaussian beam[33].

Table I. Exposure parameters used in this work. A 10 μm aperture was used in all exposures.

Pattern	Landing energy[keV]	Current [pA]	Pixel size [nm]	Dose
1 μm × 1 μm, square	29	0.7	2	70 μC/cm^2
100 μm × 100 μm, 16 nm, 50 nm	32	1.0	2	70 μC/cm^2
50 μm × 50 μm, 16 nm, 40 nm	30	1.2	2	75 μC/cm^2
50 μm × 50 μm, 16 nm, 35 nm	30	1.2	2	70 μC/cm^2
100 μm × 50 μm, tilt 45°, WD ∼ 15 mm	29	1.0	8	210 pC/cm
100 μm × 50 μm, tilt 45°, WD ∼ 27 mm	27	1.1	10	210 pC/cm

III. RESULTS AND DISCUSSION

A. Reduced proximity effects in high-density gratings

In the first experiment we demonstrate patterning of dense gratings over areas up to 100 μm × 100 μm in HIL, that is, areas much larger than the long-range scattering range (Figure 2). Dense gratings are particularly sensitive to proximity effects. To quantify the proximity effects in HIL, we exposed a 1 μm × 1 μm square in HSQ and left four windows in the center open. A substantial background dose in the unexposed regions would cause HSQ to crosslink, and hence patterning to occur outside the desired areas defined by the CAD file. The width of the windows and the gaps are found to be Figure 2(a)(top) 37 ± 2 nm and 19 ± 2 nm and Figure 2(a) (bottom) 26 ± 3 nm and 14 ± 3 nm, respectively. All windows are measured (in x- and y-direction) and the average is presented with standard deviation. The fact that the patterns almost print true to size indicates that long-range scattering is absent. The TRIM calculation[34], (Figure 2(c)), shows the trajectory of 30 keV He^+ ions into a 30 nm thick HSQ layer on 500 nm silicon. As the lateral width of the interaction volume is smaller than 1 μm, any long-range scattering effects should be present within the patterned area. It should be noted that as the resist thickness increases, ion scattering can lead to variations in dimension on the top and bottom of the exposed resist. Howevever, as indicated by the TRIM-calculation, this is not expected to be an issue for the reist thickness used here (30 nm). The deviation from the nominal size could come from the dose-tails from near-by exposure points. Winston et al. measured the point spread function of 30 keV He^+ ions and the forward scattering Gaussian distribution was found to have $\alpha = 4.1$ nm[13].

Manfrinato et al.[35] wrote an analogous square pattern in HSQ using 2 keV EBL. The electrons and the helium ions have different velocity and energy. Manfrinato et al. used a larger pixel size (10 nm) and aperture (20 μm), and a thinner resist (15 nm). Using electrons with such low energy, reduces the interaction volume, but increases the spot size of the beam. For a nominal window size of 40 nm and a gap of 40 nm, they measured the windows to have a width of 30 nm. Realizing an analogous pattern with 30 keV electrons would be extremely challenging due to the larger electron beam interaction volume, even with proximity effect corrections.

The large area gratings are presented in Figure 3 and Figure 4. In all exposures the width

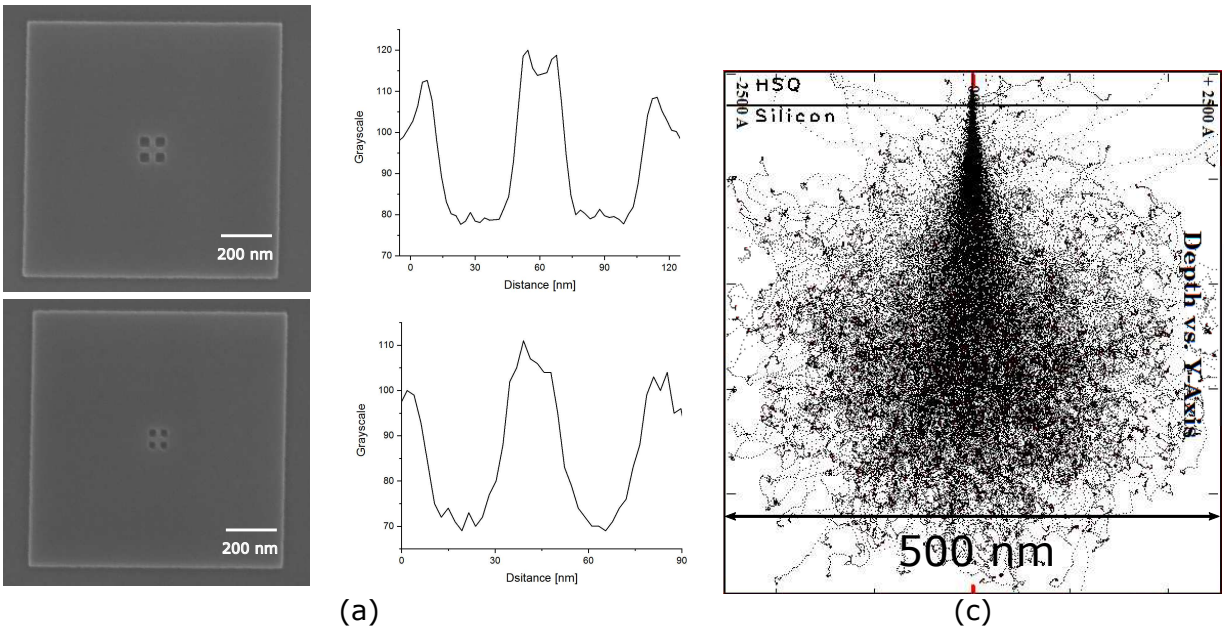

Figure 2. (a) SEM images and corresponding grayscale measurements of a 1 μm × 1 μm square in HSQ where small windows were left unexposed. In the top SEM image the windows have a nominal dimension of 40 nm and the gap between the windows is 20 nm. The width of the windows was measured to be 37± 2 nm and the gap 19 ± 2 nm. In the bottom SEM image the windows have a nominal dimension of 30 nm and the gap between the windows is 15 nm. The width of the windows was found to be 26 ± 3 nm and the gap was found to be 14 ± 3 nm. (b) TRIM calculation of the trajctories of 30 keV He^+ ions into 30 nm HSQ ($H_8Si_8O_{12}$) on silicon, showing that any effects of long range scattering should be present within the exposed area presented in (a).

of the rectangle in the CAD-file is defined to be 16 nm and the pixel size is 2 nm. The pitch is 50 nm (Figure 3), 40 nm (Figure 4(a)) and 35 nm (Figure 4(b)). The width of the lines is measured in each of the corners and in the middle of the grating and the average of 25 measurement points is presented with standard deviation. The largest area written is 100 μm × 100 μm, corresponding to the largest accessible write-field using a 2 nm pixel size. It is not a principal limitation, as discussed in Sec. II A, but because the HIM is not equipped with an interferometric stage, the largest area is limited by the pattern generator. Larger areas can be written at the cost of pixel size (resolution). The crucial point here is that a large-area, high-density pattern can be written without proximity effect corrections. There is no observable difference between the widths measured at the corners relative to the width measured in the center of the grating. If proximity effects were present, the width of lines

should change as a function of the distance to the edge of the patterned area. Furthermore, the line edge roughness of the grating is small (Figure 4). Line edge roughness depends, among others, on proximity effects and resist thickness and is therefore expected to be small for fabrication with HIL[36].

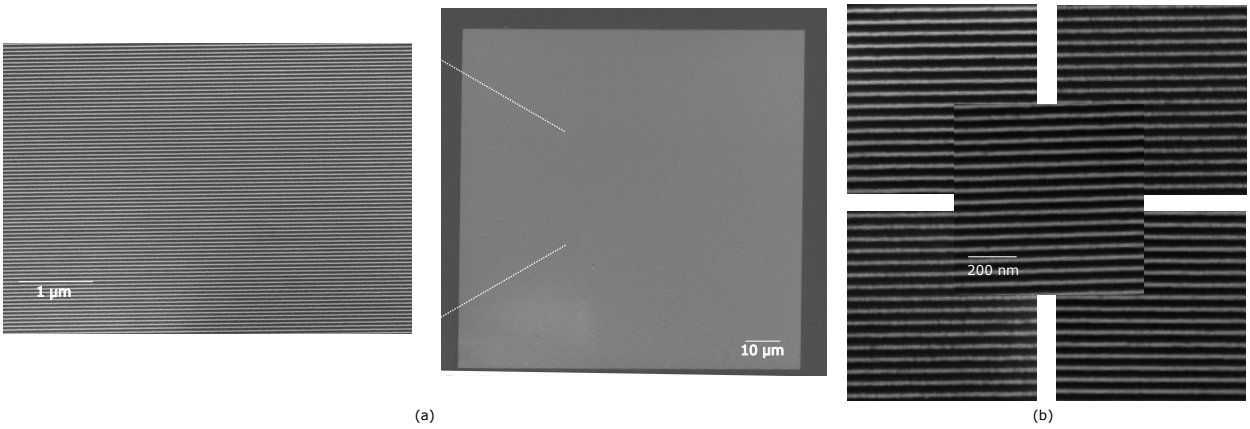

Figure 3. SEM images of a HSQ grating patterned using HIL. The lines were defined as rectangles with a width of 16 nm and pitch 50 nm. Total area is 100 µm × 100 µm. The measured width was 17 ± 1.5 nm, and the pitch was 50 ± 1 nm. The lines print true to size without any proximity effect corrections. (a) Overview SEM images (b) Close-up SEM images of the four corners and the center of the grating. The scalebar is the same for all images.

In contrast to previous work we use an area dose, instead of a single-pixel-line dose, which requires in theory a smaller dose, because the ion distribution is highly concentrated when exposing single pixels. Put in other words, when exposing a single-pixel, much of the dose is wasted by over-exposing the central region of the spot. The dose used here lies in the range 70 µC/cm^2 - 80 µC/cm^2 (corresponding to 4 ions/nm^2 - 5 ions/nm^2), see Table I. The dose-range used is about 15× smaller than a typical HSQ dose for 30 keV EBL. A significant reduction in dose relative to an electron beam of the same energy is to be expected due to the reduced interaction volume. Also, doses in the range 4 ions/nm^2 - 5 ions/nm^2, are about an order of magnitude less than the threshold at which helium ions displace and scatter atoms[37], so sputtering is assumed to be negligible. However, sub-surface damage induced by the helium ion beam, which is not taken into consideration here, could be an issue in *e.g.* electronic applications[16,37].

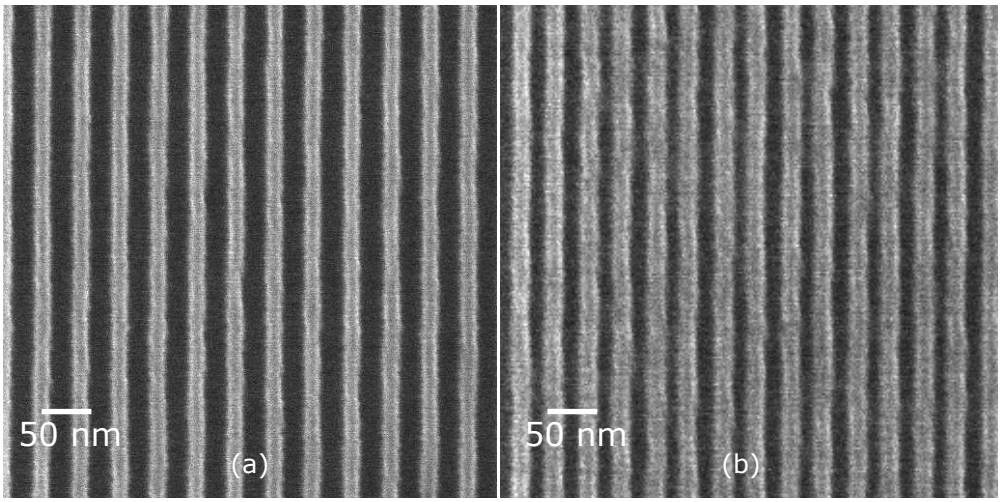

Figure 4. HIM images of a HSQ grating patterned using HIL. The lines were defined as rectangles with width of 16 nm, length 50 μm. In (a) the pitch is 40 nm. The measured width was 17 ± 1 nm, and the pitch 40 ± 1 nm. In (b) the pitch is 35 nm. The measured width is 19 ± 8 nm. The general trend is pattern collapse, likely due to overexopsure/overdevelopment.

The gratings print true to size down to a pitch of 40 nm (Figure 4(a)). The general trend for the 35-nm grating is pattern collapse, although some regions are fully developed, as can be seen in Figure 4(b). Pattern collapse often arises from overexposure/ overdevelopment, which likely is the case, and could possibly be prevented by using an even thinner resist/smaller dose/shorter development time. The linewidth distribution is found to be 19 ± 8 nm. Proximity effects should, according to what is described above and by Winston et al.[13] and Sidorkin et al.[12] not be the reason for this. Other possible reasons for pattern failure are tool optics (focus), beam current fluctuations or adsorption of adatoms near the trimer.

B. Exposures on tilted surfaces

In the second experiment we performed the first HIL patterning on tilted surfaces. We selected a reasonable resolution and did two sets of exposures. The depth of field increases for increasing working distances as the angular spread of the beam decreases. First, the beam was focused to a working distance of about 15 mm, and the sample stage tilted 45°. 100 μm single-pixel lines were patterned. As seen in Figure 5(a-c), the linewidth varies along the diagonal of the line, which serves as an estimation of the depth of field. The variation

along the first 50 μm of the line indicates that the depth of field at this resolution is smaller than 50 μm. The lines were measured along the diagonal of the grating, and the average of each region is presented. The working distance was then increased to about 27 mm and the experiment was repeated. Along the 100 μm line written, see Figure 5(d-f), the width of the single-pixel lines is found to be 26 ± 1.5 nm. This demonstrates that the depth of field for this resolution (about 20 nm) is at least 100 μm. This shows HIL's potential for patterning on tilted and curved surfaces with high resolution. Zhang et al. estimated that the depth of field for an electron beam is on the order of 10 μm[30], and hence the length scales presented here would be hard to realize using EBL without a dynamic focus correction.

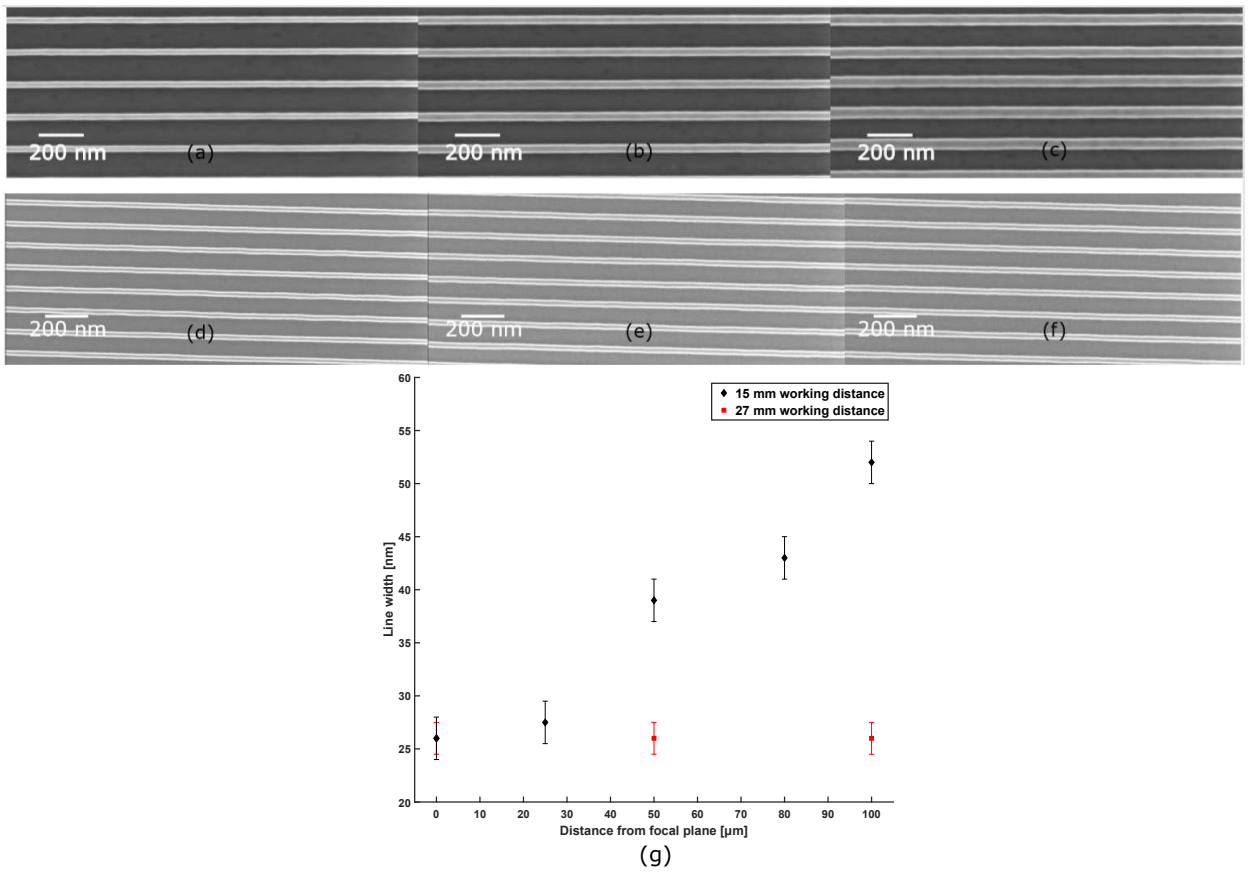

Figure 5. (a-f) SEM image along the diagonal of the 100 µm grating written in HSQ while having the sample tilted 45 °. In (a-c) the working distance was 15 mm. (a) lower left sample area linewidth 26 nm to (b) middle sample area linewidth 39 nm to (c) upper right sample area linewidth 52 nm. As the width of the lines has already changed notizably for the middle sample area, the depth of field is smaller than 50 µm. (d) lower left sample area (e) middle sample area (f) upper right sample area. The working distance used to exposure the line (d-f) was 27 mm. The width of the lines remains the same across the hole patterned area, 26 ± 1.5 nm, and therefore the depth of field for this resolution must be greater than 100 µm. (g) Plot of the linewidth versus the distance from the focal plane for a working distance of 15 mm (black) and 27 mm (red).

As an independent test, the depth of field was estimated using HIM images (see Sec. II A) for various working distances, based on the definition of defocus as described by the Rayleigh length for Gaussian beams[33]. It was found to be 12 µm ± 1 µm for 6 mm working distance, 21 µm ± 1 µm for 10 mm working distance and 29 µm ± 1 µm for 15 mm. This fits well with the exposures on the tilted sample stage.

IV. SUMMARY

In this paper we pattern high-density gratings in HSQ using HIL over areas up to 100 μm × 100 μm. The gratings are exposed using an area dose and a line width of 16 nm, and a 2 nm pixel size. We find that gratings with an area up to 100 μm × 100 μm print true to size down to a pitch of 35 nm. This would be extremely challenging to achieve with an electron beam of the same energy without proximity effect corrections. We also estimate the depth of field in the HIM for different working distances and through a series of patterns on tilted surfaces we demonstrate that HIL can be used to pattern over surface topography and on curved surfaces. Our findings show that HIL can fulfill a challenge in lithography; to print high density patterns true to size without any proximity effect corrections, while at the same time maintaining a large focus tolerance (large depth of field). This can enable high-resolution patterning of lenses or optical fibers. Future studies of the depth of field for other ion-probes, such as neon, could potentially reveal an even larger depth of field for a given spot size.

V. ACKNOWLEDGEMENTS

The authors thank Mark Mondol and Jim Daley at MIT Nanostructure Laboratory. This work was done at the MIT Nanostructure Laboratory and the MIT Scanning-Electron-Beam Lithography facility. Ranveig Flatabø gratefully acknowledges support from Bergen Research Foundation and the Norway-America Association through American-Scandinavian Foundation's The Stolt-Nilsen Fund for Education.

REFERENCES

[1]B. Ward, J. Notte, and N. Economou, "Helium ion microscope: A new tool for nanoscale microscopy and metrology," J Vac Sci Technol B **24**, 2871–2874 (2006).

[2]L. Scipioni, C. A. Sanford, J. Notte, B. Thompson, and S. McVey, "Understanding imaging modes in the helium ion microscope," J Vac Sci Technol B **27**, 3250–3255 (2009).

[3]"Microscopy and analysis," `http://www.microscopy-analysis.com/news/zeiss-smt-orion-recordresolution` (), accessed: 2017-12-01.

[4]M. Joens, C. Huynh, J. Kasuboski, D. Ferranti, Y. Sigal, F. Zeitvogel, M. Obst, C. Burkhardt, K. Curran, S. Chalasani, L. Stern, B. Goetze, and J. Fitzpatrick, "Helium ion microscopy (him) for the imaging of biological samples at sub-nanometer resolution," Sci Rep **3**, 3514 (2013).

[5]A. N. Abbas, G. Liu, B. Liu, L. Zhang, H. Liu, D. Ohlberg, W. Wu, and C. Zhou, "Patterning, characterization, and chemical sensing applications of graphene nanoribbon arrays down to 5 nm using helium ion beam lithography," ACS Nano **8**, 1538–1546 (2014).

[6]W. Vanden Berg-Foels, L. Scipioni, C. Huynh, and X. Wen, "Helium ion microscopy for high-resolution visualization of the articular cartilage collagen network," J Microsc **246**, 168–176 (2012).

[7]S. Boden, Z. Moktadir, D. Bagnall, H. Mizuta, and H. Rutt, "Focused helium ion beam milling and deposition," Microelectron Eng **88**, 2452–2455 (2011).

[8]Y. Wang, S. Boden, D. Bagnall, H. Rutt, and C. De Groot, "Helium ion beam milling to create a nano-structured domain wall magnetoresistance spin valve," Nanotechnology **23**, 395302 (2012).

[9]D. C. Bell, M. C. Lemme, L. A. Stern, J. R. Williams, and C. M. Marcus, "Precision cutting and patterning of graphene with helium ions," Nanotechnology **20**, 455301 (2009).

[10]M. M. Marshall, J. Yang, and A. R. Hall, "Direct and transmission milling of suspended silicon nitride membranes with a focused helium ion beam," Scanning **34**, 101–106 (2012).

[11]D. Emmrich, A. Beyer, A. Nadzeyka, S. Bauerdick, J. Meyer, J. Kotakoski, and A. Gölzhäuser, "Nanopore fabrication and characterization by helium ion microscopy," Appl Phys Lett **108**, 163103 (2016).

[12]V. Sidorkin, E. van Veldhoven, E. van der Drift, P. Alkemade, H. Salemink, and D. Maas, "Sub-10-nm nanolithography with a scanning helium beam," J Vac Sci Technol B **27**, L18 (2009).

[13]D. Winston, B. Cord, B. Ming, D. Bell, W. DiNatale, L. Stern, A. Vladar, M. Postek, M. Mondol, and B. K. Yang, J.K.W., "Scanning-helium-ion-beam lithography with hydrogen silsesquioxane resist," J Vac Sci Technol B **27**, 2702 (2009).

[14]H. Guo, H. Itoh, C. Wang, H. Zhang, and D. Fujita, "Focal depth measurement of scanning helium ion microscope," Appl Phys Lett **105**, 023105 (2014).

[15]R. Hill and F. Faridur Rahman, "Advances in helium ion microscopy," Nucl Instrum Meth A **645**, 96–101 (2011).

[16]W. Li, W. Wu, and R. Stanley Williams, "Combined helium ion beam and nanoimprint lithography attains 4 nm half-pitch dense patterns," J Vac Sci Technol B **30**, 06F304 (2012).

[17]X. Shi, P. Prewett, E. Huq, D. Bagnall, A. Robinson, and S. Boden, "Helium ion beam lithography on fullerene molecular resists for sub-10nm patterning," Microelectron Eng **155**, 74 (2016).

[18]D. Maas, E. van Veldhoven, A. van Langen-Suurling, P. F. Alkemade, S. Wuister, R. Hoefnagels, C. Verspaget, J. Meessen, and T. Fliervoet, "Evaluation of euv resist performance below 20nm cd using helium ion lithography," in *Proc Spie*, Vol. 9048 (International Society for Optics and Photonics, 2014) p. 90482Z.

[19]V. R. Manfrinato, A. Stein, L. Zhang, C.-Y. Nam, K. G. Yager, E. A. Stach, and C. T. Black, "Aberration-corrected electron beam lithography at the one nanometer length scale," Nano Lett (2017).

[20]T. Chang, "Proximity effect in electron-beam lithography," J Vac Sci Technol **12**, 1271–1275 (1975).

[21]G. Owen and P. Rissman, "Proximity effect correction for electron beam lithography by equalization of background dose," J Appl Phys **54**, 3573–3581 (1983).

[22]E. Dobisz, C. Marrian, R. Salvino, M. Ancona, F. Perkins, and N. Turner, "Reduction and elimination of proximity effects," J Vac Sci Technol B **11**, 2733–2740 (1993).

[23]N. A. Melosh, A. Boukai, F. Diana, B. Gerardot, A. Badolato, P. M. Petroff, and J. R. Heath, "Ultrahigh-density nanowire lattices and circuits," Science **300**, 112–115 (2003).

[24]J. Henzie, J. Lee, M. H. Lee, W. Hasan, and T. W. Odom, "Nanofabrication of plasmonic structures," Annu Rev Phys Chem **60**, 147–165 (2009).

[25]D. Winston, J. Ferrera, L. Battistella, A. Vladar, and K. Berggren, "Modeling the point-spread function in helium-ion lithography," Scanning **34**, 121–128 (2012).

[26]"Zeiss," `https://www.zeiss.com/microscopy/int/products/multiple-ion-beam/orion-nanofab-for-materials.html` (), accessed: 2017-12-10.

[27]J. H. Burge, D. S. Anderson, T. D. Milster, and C. L. Vernold, "Measurement of a convex secondary mirror using a holographic test plate," in *P Soc Photo-Opt Ins*, Vol. 2199 (International Society for Optics and Photonics, 1994) pp. 193–199.

[28]Y. Xie, Z. Lu, and F. Li, "Fabrication of large diffractive optical elements in thick film on a concave lens surface," Optics exp **11**, 992–995 (2003).

[29]A. del Campo and C. Greiner, "Su-8: a photoresist for high-aspect-ratio and 3d submicron lithography," J Micromech Microeng **17**, R81 (2007).

[30]J. Zhang, B. Shokouhi, and B. Cui, "Tilted nanostructure fabrication by electron beam lithography," J Vac Sci Technol B **30**, 06F302 (2012).

[31]B. Farshchian, A. Amirsadeghi, S. Hurst, J. Wu, J. Lee, and S. Park, "Soft uv-nanoimprint lithography on non-planar surfaces," Microelectron Eng **88**, 3287–3292 (2011).

[32]J. Yang and K. Berggren, "Using high-contrast salty development of hydrogen silsesquioxane for sub-10-nm half-pitch lithography," J Vac Sci Technol B **25**, 2025 (2007).

[33]H. E, *Optics 4 Edition* (Addison-Wesley, 2001).

[34]J. Ziegler, J. Biersack, and M. Ziegler, "SRIM -The stopping and range of ions in matter," MD: SRIM Co., 2008.

[35]V. R. Manfrinato, L. L. Cheong, H. Duan, D. Winston, H. I. Smith, and K. K. Berggren, "Sub-5kev electron-beam lithography in hydrogen silsesquioxane resist," Microelectron Eng **88**, 3070–3074 (2011).

[36]S. Eder-Kapl, H. Loeschner, M. Zeininger, W. Fallmann, O. Kirch, G. P. Patsis, V. Constantoudis, and E. Gogolides, "Line edge roughness investigation on chemically amplified resist materials with masked helium ion beam lithography," Microelectron Eng **73**, 252–258 (2004).

[37]R. Livengood, S. Tan, Y. Greenzweig, J. Notte, and S. McVey, "Subsurface damage from helium ions as a function of dose, beam energy, and dose rate," J Vac Sci Technol B **27**, 3244–3249 (2009).